# THE COMPACTION OF RAPIDLY SOLIDIFIED MATERIALS

H. FISCHMEISTER and E. ARZT
MPI für Metallforschung
Institut für Werkstoffwissenschaften
D-7000 Stuttgart, F.R. Germany

## 1. INTRODUCTION

Powder compaction has two equally important aspects: the elimination of pores and the creation of bonds between the particles. Important bonding mechanisms are cold welding and mechanical interlocking of particle surfaces. The first requires plastic flow in order to break the surface oxide, the second depends on irregular surface geometry. Hard, smooth particles do not usually permit the action of either of these mechanisms; after compaction, they simply fall apart again. Such powders must be contained in capsules and, after compaction, must be bonded by sintering or hot pressing. This has in fact become the normal fabrication route for superalloy and tool steel powders.

Powders of rapidly solidified metals are either obtained as spherical particles, by solidification of melt droplets, or in the form of flakes or splat, or by the mechanical comminution of ribbons (usually after embrittlement). All of these belong to the difficult-to-bond category, and they tolerate only limited heating without loss of the special properties for whose sake the rapid solidification process was used. Consequently, hopes and efforts have been directed at developing thermomechanical treatments which provide enough force for complete densification with limited heat exposure - either in the direction of "warm" (as opposed to hot) working, or in the direction of very fast ("dynamic") compaction with high energy input.

Regarding their heat tolerance, rapidly solidified materials can be divided into two categories: those whose properties depend on the amorphous or microcrystalline state, and those which merely rely on a high degree of solid supersaturation for subsequent precipitation hardening. The latter are less sensitive, especially if the heating suffered during consolidation can be utilized for the precipitation treatment. The former category, however, appears more exciting because its property potential in the compacted state is as yet virtually unexplored. Here, dynamic compaction is of particular interest because it has been found that, in favourable circumstances, the particles are bonded by a thin layer of melt which freezes rapidly enough to become amorphous or microcrystalline, without serious property degradation in the interior of the particles. It is difficult, however, to achieve this favourable combination of circumstances throughout the volume of the compact and to obtain complete densification at the same time. "Warm" working, while less powerful, is easier to control.

In the first part of this paper, the theory of the compaction of particle systems will be reviewed; in the second, techniques of dynamic compaction. The third part discusses particle bonding, and the final sections deal with the problem of processing windows for dynamic and "warm-slow" compaction.

## 2. A MODEL FOR THE COMPACTION OF SPHERICAL POWDERS

The compaction behaviour of powders is usually characterized by plotting the pressure required to achieve desired density levels. These curves have an unexciting shape and are easily fitted by combinations of simple functions with adjustable parameters. Such fit formulae are reviewed in references (1) to (4); we will pass them by because they do not contribute to physical understanding.

A useful descriptor for the progress of compaction is the relative density, D, normalized to the density (m/v) of the pore-free material:

$$D = \frac{(m/v)_{\text{porous compact}}}{(m/v)_{\text{pore-free-material}}} = \frac{v_m}{v_m + v_p} \qquad (1)$$

(v = volume; m = mass; indices: m = 'material', p = 'pores')

The relative density is directly related to the volume fraction of pores, or void fraction, V:

$$V = 1 - D \qquad (2)$$

The first rational model of the compaction process was based on the idea that compactability is proportional to the void fraction (5) and (6):

$$\frac{dV}{dP} = \beta V \qquad \text{with P = pressure} \qquad (3)$$

Integration leads to

$$P = \frac{1}{\beta} \ln \frac{V_0}{V} \qquad \text{with } V_0 = \text{void fraction in uncompressed powder.} \qquad (4)$$

It is interesting to note that the same expression is obtained when the compaction process is modelled by the plastic collapse of a hollow sphere, with a volume ratio of void-to-shell equal to that of pores-to-solid in the powder compact (7).

Equation 4 describes the compaction behaviour of many powders in a limited range of pressures, relevant for the molding of sintered parts (which have about 15% porosity), but the agreement turns out to be fortuitous. The constant $\beta$ is inversely proportional to the flow stress of the particle material, but the factor of proportionality derived from the hollow-sphere model is wrong by a factor of 4.5.

Later work (4),(8)-(12) has shown that the compaction of a powder mass has three stages:

(i) TRANSITIONAL RESTACKING - reduction of the total pore volume by sliding of particles past each other; this is brought to an end by the frictional locking of particle contacts as the pressure increases. It has been shown that restacking plays only a minor role in the compaction of spherical, deformable powders (12).

(ii) PLASTIC DEFORMATION AT PARTICLE CONTACTS (figure 1). This mechanism predominates until the porosity has been brought down to slightly below 10% (13). From then on, it is increasingly replaced by

(iii) PLASTIC COLLAPSE OF RESIDUAL PORES entirely surrounded by solid.

An exact model has been constructed for the second stage, figure 1a and b, and combined with an approximate model for the third stage (13). An important feature is the increase of the number of particle contacts as all particles are brought closer together, cf. figure 1c. This can be described (14) by recourse to the radial distribution function (RDF) of the particle packing. The RDF of a random close packing of spheres of equal size is well known (15); within the narrow interval of interparticle distances of interest, it can be replaced by a linear term (figure 1d).

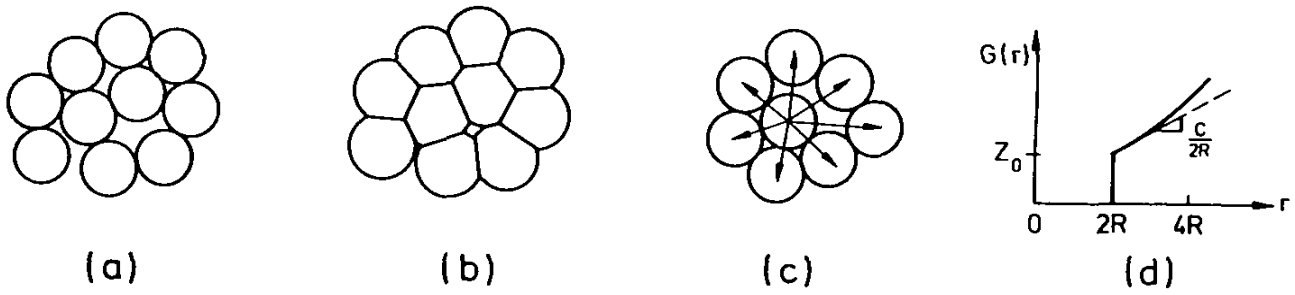


Figure 1: Compaction of spherical particles by plastic deformation at contact points (a,b). New contacts are created at a rate depending on the radial distribution function of the particle packing (c,d).

As far as the forces active in compaction are concerned, a powder compact can be viewed as a network of lines linking the particle centers. An isostatic compaction pressure will tend to shorten all these links. Each link resists shortening with a force which depends on the flow stress of the material, $\sigma_f$ , and the size of the contact area, a, in a manner which can be modelled on the known force law of a spherical indenter entering a flat plate,

$$f = 3\ \sigma_f\ a \tag{5}$$

If there are Z contacts per particle, the equilibrium between the applied pressure and the forces opposing it can be written

$$P = \frac{3}{4\pi R^2}\ \sigma_f\ D\ a\ Z \qquad (R = \text{particle radius}) \tag{6}$$

The quantities a, Z, and $\sigma_f$ are all functions of the density achieved. In particular, the number of contacts per particle, Z(D), increases steadily as the densification progresses. This, and the average size of the contact flats, a(D), can both be calculated from the RDF of the powder packing (13,14). To calculate $\sigma_f$, the average strain in the contact region - which, with given RDF, can again be expressed as a function of density - is inserted into the strain hardening law of the particle material (13).

In stage (iii), an additional term is introduced to model the contribution of entirely surrounded pores to the densification resistance, using weight factors $f_h$ and $f_s$ for the volume fractions of "hard" regions (where the pores are closed) and "soft" regions (where densification still proceeds by flattening of non-contiguous particle contacts). These volume fractions, too, are functions of the packing geometry and the instantaneous density.

The complete compaction formula which results from this treatment,

$$P = \sigma_f(D)\left[f_s\ (D)\ \frac{3}{4\pi R^2}\ (aZ)_D\ D + f_h\ (D)\ 2\ell n\ \frac{(aZ)_{D=1}}{(aZ)_{D=1} - (aZ)_D}\right] \tag{7}$$

contains only material constants in the term $\sigma_f(D)$ and only geometrical quantities - all emanating from the RDF - in the brackets. This allows a unified description of the pressure - density relation for spherical powders of plastically deformable materials which is in good agreement with experimental data, without recourse to arbitrarily adjustable parameters.

The model has been derived for monosize spheres. In real powders, the particles have a size distribution, allowing smaller particles to be stacked in the interstices between the larger ones. This will increase the average number of particle contacts, but at the same time, the average size of the contact flats will decrease. Measurements by quantitative metallography on compacts made of powders with a very narrow and a normal size dispersion have shown (13) that the product (a·z), which is the essential variable in equations 6 and 7, is very little affected by the size dispersion. The main effect of the size dispersion is on $D_0$, the density of the uncompacted powder. In fact, it has been found (13), (16), that equation 7 satisfactorily describes the compaction of moderately non-spherical powders as well. Systematic deviations occur during the phase of transitional restacking, figure 2, and their extent correlates clearly with the deviation from sphericity. In the context of rapidly solidified materials, the model is certainly applicable to melt droplets solidified in free flight, and to powders obtained by mechanical comminution of embrittled ribbons.

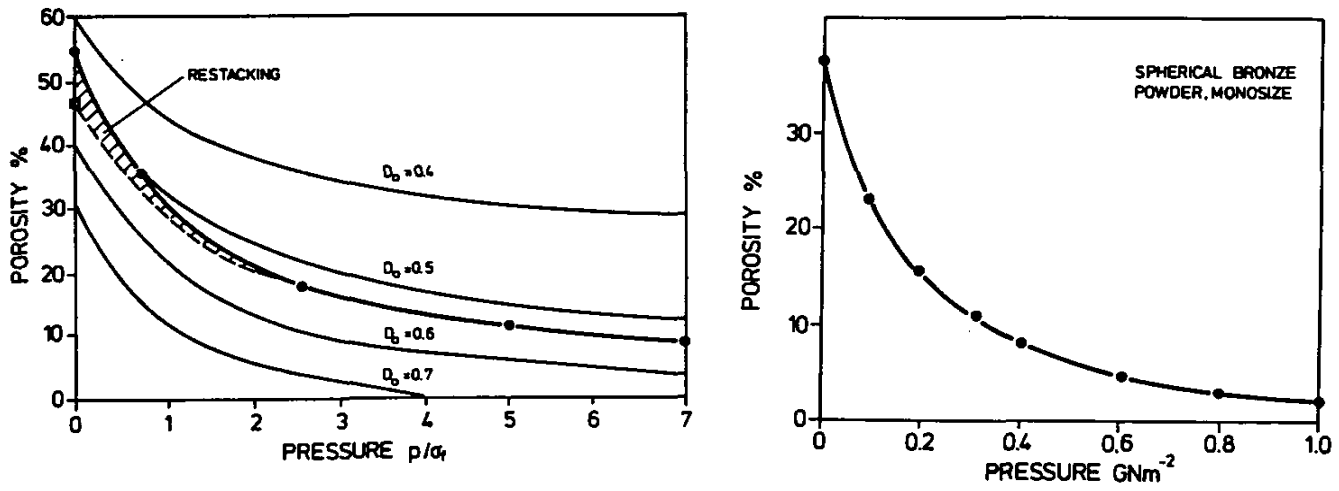


Figure 2: (a) The compaction of spherical bronze powders conforms to equation 7. (b) Non-spherical powders have different initial densities $D_0$. In a net corresponding to equation 7, with $D_0$ as a parameter, the compaction of non-spherical zinc powder is seen to conform to equation 7 except in the phase of restacking.

In equation 7, the first term in brackets reflects the fact that in stage (ii), the compaction force is being opposed by an increasing number of particle contacts, with increasing contact areas. This effect has been termed "geometrical hardening" of the powder compact (13). The second term, which comes into play when the relative density exceeds 92 %, describes the rapid increase of the system's resistance to compression as more contact flats impinge on each other, sealing off the pore they surround. While in stage (ii), the flow of material from the contact region into the void space is essentially unconstrained, strong plastic constraints come into

play in stage (iii), which therefore has been termed the stage of constraint hardening of the compact. As a result, the resistance to compression mounts rapidly and, in fact, becomes infinite as the pore size and thus the void fraction goes towards zero. This is reflected by the logarithmic term in equation 7. If only the final stage is considered, equation 4 would provide an alternative and formally similar description. Both descriptions allow only an asymptotic approach to full density, which is in full agreement with practical experience.

Arzt, Ashby and Easterling (17) have considered densification by thermally assisted mechanisms, i.e. power law creep and diffusion, with regard to hot isostatic pressing. In the present context, power law creep is of greater interest. Based on a solution for the creep rate of a thick spherical shell surrounding a central void, the following densification rate is obtained for the final stage:

$$\dot{D} = \frac{3}{2}\dot{\varepsilon}_o \frac{D(1-D)}{[1-(1-D)^{1/n}]^n}\left[\frac{3}{2n\sigma_o}\left(P+\frac{2\gamma}{r}\right)\right]^n \qquad (8)$$

with $\dot{\varepsilon}_0$, $\sigma_0$, n = power law creep parameters; $\gamma$ = surface energy; r = pore radius.

For property-relevant porosities, where the pores are still large enough to allow the surface energy term to be neglected, this becomes

$$\dot{D} = \text{const} \cdot V \cdot P^n . \qquad (9)$$

indicating that the pressure required to uphold a desired densification rate rises with the nth power of inverse void fraction (n=4 is a common value). Complete elimination of pores, therefore, is only possible by sintering with surface energy as the driving force.

## 3. DYNAMIC COMPACTION

The early development of dynamic powder compaction methods has been reviewed by Clyens and Johnson (19). Important early variants were the Dynapak, a pneumatic high-speed press; the petroforge, a piston machine actuated by ignition of a fuel-air-mixture; various devices for magnetic compaction with strong current pulses, and explosive-driven fluid-dynamic and ballistic presses. To these might be added conventional equipment for moderate-rate metal forming, like forging hammers and extrusion presses. A new regime of much higher compaction rates was opened up by direct explosive compaction, with explosive in direct contact with the powder (e.g., in the form of concentric tubes). This technique is widely practiced (18)-(21), in particular for brittle materials like ceramics (22),(23). In this case, its success is at least partly due to the generation of a high dislocation density in the powder, which makes the material more amenable to densification by sintering. However, the method has also been successfully applied to amorphous metals (24), where subsequent sintering plays no role. The latest development is a ballistic gas gun which projects a flier plate at high velocity against the powder, achieving compaction rates similar to those of direct explosive compaction, while allowing closer control of the energy transfer to the powder (25) to (27).

Table I compares characteristic compaction rates.

Typical platen speeds in the Dynapak and Petroforge units were of the order of 20 m/s; with the Raybould gun, flyer plate velocities up to 2500 m/s have been achieved (29); effective pressures in the powder mass are typically in the range from 2 to 5 GPa, but experiments up to 18 GPa

Table I: Compaction Rates in Various Processes

| | |
|---|---|
| Extrusion press | 50/s |
| Forging hammer | 100/s |
| Dynapak, petroforge | 10-100/s |
| Explosively pressurized fluid-dynamic press | 10-100/s |
| Magnetic compaction | 20-100/s |
| Explosive ballistic compaction | 200-500/s |
| Direct explosive compaction | 1000-10.000/s |
| Two-stage air gun | 1000-10.000/s |

have been reported (26). For comparison, typical compaction pressures in powder metallurgy production are of the order of 0.5 GPa. - The range of typical pressures and shock velocities obtained with these guns is similar to those which occur in direct explosive compaction of powders (20)-(22). The shock waves induced in the powder by such high-velocity impact produce effects which cannot occur at the modest speeds of the earlier "dynamic" devices, and their utilization has opened a new era of dynamic powder compaction.

At high rates of deformation, the flow stress of metallic materials increases drastically (30). Strain rates of $10^7$ - $10^8$ $s^{-1}$ have been claimed for dynamic compaction experiments with a stainless steel powder (31). Extrapolating from what is known from static compaction experiments (12), this should lend much greater importance to the stage of restacking by particle sliding. Even in the regime of conventional static pressures, faster compaction rates have been found to improve interparticle bonding, as reflected by electrical conductivity and strength of the unsintered compacts (19); also it has been observed that interparticle friction in powders increases significantly under dynamic loading (19). These effects all point to more efficient break-up of surface contamination as the particles slide quickly past each other.

At the very high speeds now coming into use, strong heating at the particle surfaces is observed, while the particle interiors stay relatively cool. Figure 3, reproduced from the work of Morris (32) on a 0.5 % carbon steel powder, demonstrates this convincingly by the etch-resistant martensite zones formed at the periphery of the particles as the material cools down from the temperature attained during shock compaction. The particle interior acts as a heat sink, removing the heat fast enough to quench the periphery from the austenitic to the martensitic state. As the shock pressure is raised beyond 4 GPa, regions of rapidly-solidified melt appear at the particle junctions, indicating a still higher degree of surface heating. Similar melt zones are claimed to occur in explosive welding (33). For steel powders compacted with a shock velocity of 1 km/s (shock pressure 6 GPa), Morris (34) has calculated a surface power density of $10^{11}$ $W/cm^2$, more than enough to produce melting at the particle surfaces. Interparticle melting has been observed with powders of widely different materials (35) such as lead (25), tool steels (28). Ni-base superalloys (24), (32), (34), stainless steel (31), aluminium alloys (34) and metallic glasses (35), (36). The structure of the interparticle melt region is either a microcellular solidification structure, or it may be amorphous. A cooling rate of $10^{10}$ K/s has been calculated from the surface heat input, assuming ideal heat transfer to the particle interior, and rates in the range $10^5$ -$10^{10}$ K/s have been inferred from the cell dimensions (28), (34), (36).

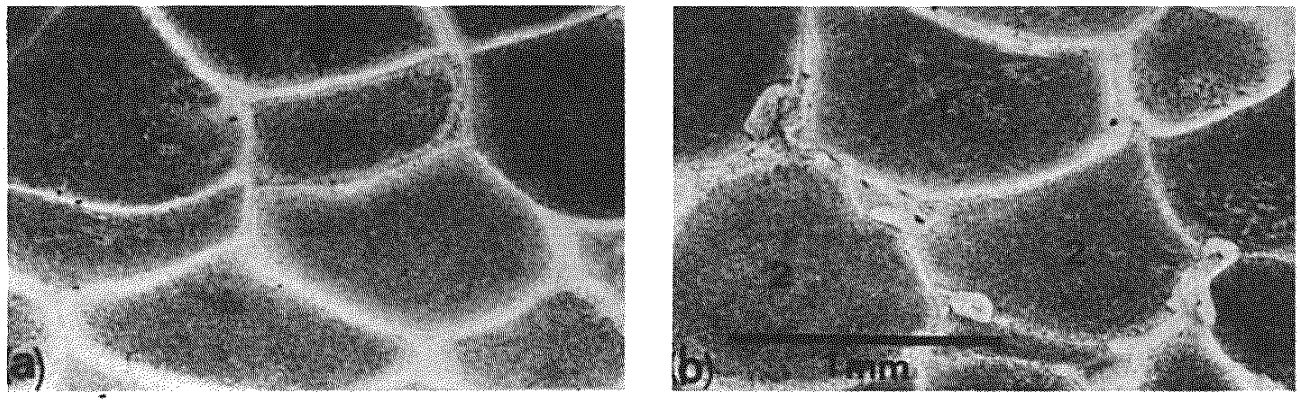


Figure 3: White-etching martensite outlines zones of adiabatic heating in tool steel powder (a) 3 GPa, (b) 5.5 GPa, with melt pool between particles 1 and 2. Micrographs from Morris (32).

Several reasons may account for the concentration of adiabatic heating at the particle surfaces: sliding friction in the first stage of the compaction process; the plastic work done in deforming the contact zones in the second stage; finally, it has been pointed out (24) that when a particle is traversed by the shock front, immediate lateral release occurs at the particle surfaces, transforming the shock wave into a plastic wave at the particle surfaces and slowing it down. This effect is proportional to the square root of the work hardening rate, which may account for material-dependent differences in consolidation behaviour. Judging from the deformation mechanism maps for high strain rates developed by Sargent and Ashby (37), deformation of the particle surfaces in dynamic compaction must occur by adiabatic shear, which would help to explain the localization of heating to the contact zones.

In the light of the densification models discussed above, a strictly local heating of the particle surfaces is the most economical way of using heat to assist the compaction of metastable materials, because it produces softening only where it is required, without superfluous heat input that might jeopardize the metastable structure in the interior of the particles. The effect of adiabatic surface heating on densification is demonstrated very clearly in figure 4, from the work of Raybould (31). Later measurements with less scatter (35) indicate that the elimination of the last fraction of porosity may be asymptotic also in dynamic compaction, but at least a practically satisfactory density of, say, 99 %, is achieved more easily than in the static mode.

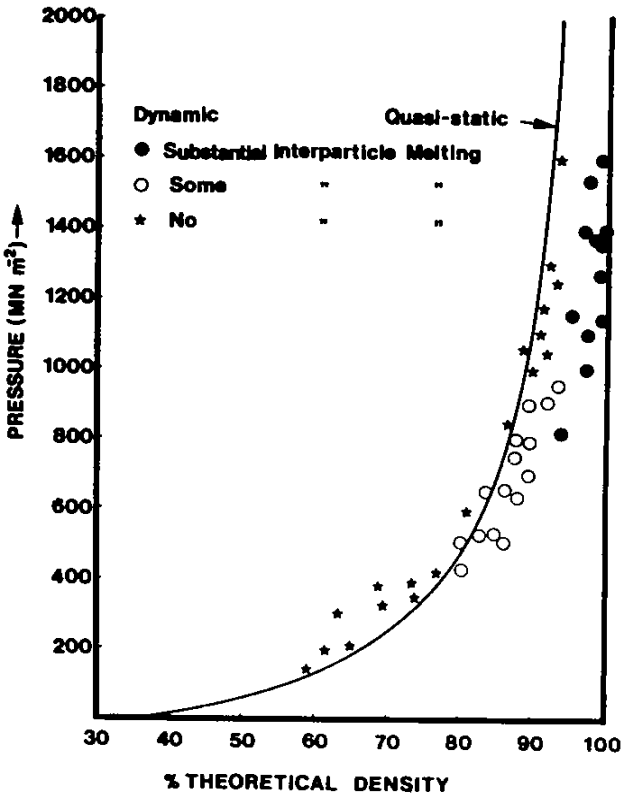


Figure 4: Pressure-density relationship for stainless steel powders, for static and dynamic compaction. Adiabatic heating of particle surfaces facilitates the approach to full density (31).

## 4. BONDING

In ordinary powder metallurgy, bonding is initiated by cold welding at deformed particle contacts and completed by diffusional mass transport during sintering. If metastable materials are to be consolidated, ordinary sintering treatments are excluded because less atomic transport is necessary for crystallization than for bonding. Thus, bonding has to be achieved, and perfected, at the moment of consolidation.

Obstacles to bonding are oxide films and other kinds of non-metallic contamination at the particle surfaces. Recent studies of early stages of wear (38) have shown that metallic bonds are formed immediately when two sputter-cleaned metal surfaces are put in touch with each other in an ultra high vacuum; similar observation have been reported for such dissimilar material pairs as copper on alumina (39). The classical work of Bowden and Tabor (40) has made it clear that metallic adhesion at oxidised surfaces is favoured when a brittle oxide is present on an easily deformable substrate, and it has been amply demonstrated that sliding or shear deformation will disrupt oxide films and produce cold welding where mere unidirectional pressure will not. Frictional heating at rubbing asperities facilitates the deformation of the substrate, and may in fact cause surface melting. Since oxides mostly remain brittle up to the melting temperatur of their substrate metal, the thermal softening of the substrate will greatly facilitate the disruption of the film. Once metallic bonding has been achieved at points, it is assumed that the oxide is stripped and rolled up or otherwise transformed into a shape in which it does not severely weaken the bond. The fact that friction welding is fully established as an industrial production process demonstrates the reliability with which bonding obstacles can be overcome by surface shear.

In the field of superalloys, unsatisfactory strength of the interparticle bonds has long been a problem - and this in spite of the fact that ample time and heat for diffusional bonding is available here. In this case the

problem lies in the segregation of impurity elements and in the precipitation of carbides at the particle boundaries during the thermal cycle connected with the consolidation process. For a long time, therefore, there was a tendency to avoid using HIP ped material without additional hot working which was meant to improve bonding by shear deformation. In reality, the shear deformation only produces a more pleasing microstructure, by destroying the particle outlines; to some degree, it may also facilitate the collapse of residual pores. While opinions in the industry are still divided, many technologists now agree that fully satisfactory properties can be obtained by HIP treatment without subsequent forging, provided the particle surfaces are kept clean of external oxide, segregated impurities from the interior, and carbides precipitated during the HIP treatment. This is possible by good hygiene during atomization and handling, cleanliness of the melt, and proper temperature-time-pressure profiles for the HIP operation. In the context of dynamic compaction, we can first of all discount diffusional reactions (segregation, precipitation) at the particle surfaces as obstacles to bonding. The destruction of oxide films by sliding will depend on their thickness and mechanical stability, and will be assisted, as discussed above, by heating at the particle contacts.

Of the many reports on dynamic compaction of powders, only a few have assessed the degree of bonding by mechanical measurements. Ultimate tensile strength and elongation at fracture are sometimes stated (29), (31), (41), but they are sensitive to residual porosity, which makes them poor indicators of bonding. Bonding per se is much better reflected by fracture toughness, especially when combined with SEM fractography to assess the frequency of interparticle fracture. Fracture toughness data have been reported by Morris (35), (42), (43) for a number of materials, including two metallic glasses. The most complete set of data is available for a soft annealed high speed steel powder (figure 5). For this material (which is not amorphous), both density and fracture toughness are seen to approach satisfactory levels only at shock pressures where sizeable amounts of interparticle melt are formed. For his amorphous materials, Morris only states a "pressure for good bonding", which is at least equal to but often in excess (by 20-200 %) of that required to reach 99 % density. Most observers have associated "good bonding" with interparticle melting. The association is sometimes backed up by a purported analogy with explosive welding of plates, where liquid jets are supposed to clean the mating surfaces. It should be pointed out, however, that causality has not been proven: the simultaneous occurrence of melt and bonding might in truth be independent effects of the particle strain rates induced. The authors of a paper on dynamic compaction of a low alloy, 0.1 % carbon steel powder (29) state emphatically that interparticle melting is required for good bonding (44), yet the microstructures reproduced show no evidence of melting, only a general homogenization at higher shock presssures. Very recently, Morris (41) has published results of warm compaction tests with a devitrified Ni-Si-B glass in which slow uniaxial hot pressing was combined with some shear deformation, and of forging tests involving a certain shear component. The densities and strengths obtained were superior to those of dynamically compacted specimens. Bonding is attributed to sufficient interparticle shear for the disruption of oxide films. The shear-pressing experiments were carried out under a protective atmosphere; no data are given for the forging tests.

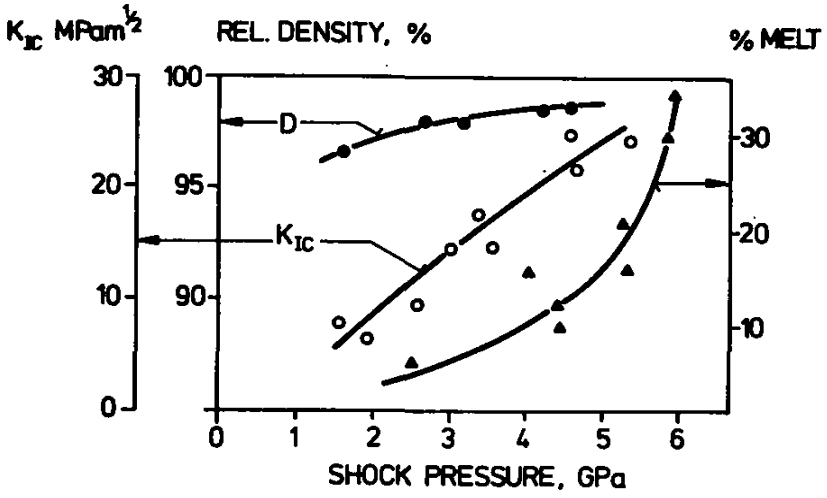


Figure 5: Density, fracture toughness and volume fraction of melt in dynamically-compacted tool steel powder of type M2, vs. shock pressure *)(data from Morris, ref. 35).

It is not a priori certain that a melt must produce an optimum bond between two solid surfaces: bonding defects are a frequent, sad experience both in soldered joints and in fusion welds; solid-solid sliding, on the other hand, demonstrates its power for bonding painfully in many a wear couple. Morris (35) states that the molten material which is squeezed into the pores "often does not bond well". At present, there is simply too little information to identify the actual bonding mechanism acting in dynamic compaction.

Surprisingly, no attention seems to have been given to all-inert-gas-processing of glassy metals; such processing routes are used for, e. g., superalloys to ensure particle cleanliness of a degree which allows perfect bonding. At least it would be worth while to find out whether the surface oxide on amorphous metal particles can be so reduced as to facilitate bonding at the more easily controlled strain rates of warm forming.

Another possibiltiy of consolidating amorphous metal particles would be sintering with a low-temperature liquid phase which perhaps could be absorbed in the amorphous material after it had promoted densification and bonding. Such transient liquid phase sintering is used, e. g., in the consolidation of dental amalgams at ambient temperatures, and can be combined with the forging of powders (45).

---

*) The data for volume fraction of melt in figure 5 may not be truly representative: with comparable energy input ( = equalized temperature of the compact after the shot), all other materials studied by Morris uniformly show about 10% less melt than the tool steel. With this material, it is not trivial to distinguish rapidly-solidified melt from quenched solid austenite; alternatively, special behaviour might be caused by the material's pronounced work hardening.

## 5. PROCESSING WINDOWS FOR DYNAMIC COMPACTION

A window for the dynamic compaction of amorphous metals will be limited by the following considerations (35,44):

(i) sufficient shock pressure to produce high density ($\geq$99%);

(ii) sufficient shock pressure to produce reliable bonding;

(iii) the interparticle melt must have time to solidify and become strong before it is reached by the descending flank of the shock pulse (which acts as a rarefaction wave);

(iv) reflection of the shock wave into the compact must be avoided;

(v) after temperature equalization on the scale of a particle diameter, the temperature must be low enough to avoid crystallization or other kinds of property degradation of the amorphous material.

Each of these points has its problems.

"Full density" is reported in many papers on dynamic compaction, but the reliable achievement of close-to-zero porosity throughout each specimen in a series of equal shots still seems to be problematic as can be seen from figure 4; elsewhere, density variations of ca. 2 % were stated for "fully dense" dynamically compacted material (29). It must be remembered that porosity of the order of 1 % generally has a strongly adverse effect on ductility (fracture strain), impact and fatigue strength of consolidated powder bodies.

The topic of bonding will not be resumed here.

The duration of the shock pulse can be controlled via the thickness of the flier plate; reflection of the shock wave can be prevented by momentum traps, e.g. a loosely attached spall plate or an absorber piston at the base of the target assembly (29),(46). In direct explosive compaction with the commonly preferred, concentric-cylindrical assembly, shock wave interaction at the center is less easily controlled and can cause blow-out of the core.

Schwarz et al. (44) have presented the following estimates for the compaction of a low alloy steel powder:

Table II: Typical time parameters in dynamic compaction.

| | |
|---|---|
| Duration of shocked state | 2 µs |
| Densification and interparticle melting | 40 ns |
| Solidification of interparticle melt | 200 ns |
| Temperature equalization between particle surface and interior | 10 µs |
| Relaxation to ambient temperature | 5 ms |

(Times greater by two orders of magnitude have been stated by Morris (28) for (larger?) specimens of dynamically compacted tool steel).

Equating the bonding criterion (ii) with the production of 10 v/o interparticle melt, and combining it with the shock duration criterion (iii), Schwarz et al. (44) have constructed the consolidation map shown in figure 6, where the normalized coordinates are

energy input: $$\epsilon = (Pv_p/2)/(\bar{c}_p(T_m - T_o)) \quad (10)$$

and shock duration $$\tau = 16\, D_m t/R^2 \quad (11)$$

($P$ = shock pressure, $v_p$ = volume of pores in unit mass of powder, $\bar{c}_p$ = average specific heat, $T_m$ = melting temperature, $T_o$ = initial temperature, $D_m$ = thermal diffusivity of particle material, $R$ = particle radius).

It will be noted that the latent heat of melting is neglected in the denominator of equation 10 which should be the total specific heat content of the particle material at the melting temperature. No attention is paid to property degradation during cooling after the shot.

Morris (35) has studied the criterion for property degradation (v). In small specimens (25 mm diameter x 10 mm high) of compacted Metglas, crystallization was observed at prior particle boundaries when the specimen temperature after the shot exceeded 450°C. His graphs show that this temperature was reached when as little as 1-2 % of interparticle melt had formed during compaction, and he concludes that "the window for compaction of highly metastable materials is a very narrow one". In figure 6, the upper energy limit ($\epsilon$=1) is for total melting of the compact. For degradable materials, the limit would be much lower, and it would move further to lower energies with increasing compact size because of slower heat extraction after the shot. Morris' observation of degradation at 1-2 % melt would make the window in figure 6 negative. It is doubtful whether a positive window exists for compacts beyond the button-size which is characteristic of the present state of the art.

Experiments in dynamic compaction mostly seem to have been limited to densification studies, and there is hardly any detailed information on the state of the compacted specimen. Only Roman et al. (36) have reported radial distribution functions which show some sharpening of the peaks at flier plate velocities above 900 m/s. This is interpreted as indication of "some ordering of the structure" under the influence of the thermal effects of the shock.

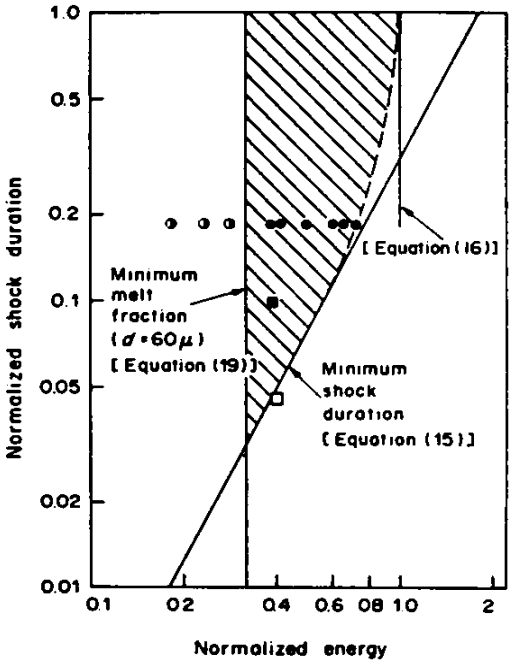


Figure 6: Dynamic consolidation map, after Schwarz et al.,(44). Data points for low alloy steel powder - solid circles: compacts with good strength; half filled circles: poor strength; open square: poor strength due to microcracks. The asymptotic limit at $\epsilon$ = 1 corresponds to total melting of the powder. Successful consolidation of this powder is expected within the shaded area.

## 6. PROCESSING WINDOWS FOR SLOW WARM CONSOLIDATION

By most accounts, the reliable attainment of homogeneous high density in dynamic pressing is still problematic, and the process is limited to very simple shapes. Slower methods like extrusion or uniaxial or isostatic pressing would appear to be more easily controllable and more versatile. Is it possible to find a processing window where full densification can be achieved without devitrification? Published experiments are few, but they offer some encouragement.

The "warm" range is limited, on the one hand, by the transition at $T_p$ from shear band to homogeneous deformation, where the materials begin to show some ductility and on the other hand, by the glass transition temperature $T_g$. For the popular alloy type $Fe_{40}$-$Ni_{40}$-$B_{20}$, $T_p$ = 470 K, $T_g$ = 715 K, but for many other amorphous alloys, $T_p$ is of the order of 550 K (47). Thus "warm" will often mean ca. 280-450°C.

Liebermann (47) obtained fully dense specimens with fair interparticle adhesion by warm extrusion of $Fe_{81.5}$-$B_{14.5}$-$Si_4$ at 640 K; uniaxial pressing at 660 K of a similar alloy resulted in 96 pct density at a pressure of 2GPa, but poor adhesion. Full densification is also reported for $Cu_{60}$-$Zr_{40}$ after extrusion close to the glass temperature (48). Uniaxial compaction of $Ni_{80}$-$P_{20}$ at constant pressure and heating rate has been studied by Bruson and Maloufi (49) who achieved densities as high as 90 % at only 200°C and 0.8 GPa; the experiments were not extended to higher temperatures, although a tendency for improvement is clearly suggested. The same tendency was observed in warm pressing experiments with $Cu_{60}$-$Zr_{40}$ (50). A review paper by Miller (51) mentions several examples of successful warm consolidation of amorphous powders, especially at temperatures close to the glass transition (48),(52),(53).

Some property degradation probably occurred in most or all of these experiments, but little information is given. In addition to incomplete densification and bonding, in any warm-slow process one would have to beware of embrittlement and partial crystallization. Magnetic properties of warm consolidated materials generally indicate structural relaxation (51), but in one instance, high temperature forming has been reported to produce no significant loss in magnetic properties (54).

Data from Morris (41) for $Ni_{70}$-$B_{20}$-$Si_{10}$ compacted by a variety of techniques at temperatures far above the truly "warm" range are reproduced in figure 7. The data are shown here to illustrate the difficulty of full densification even at temperatures where the material must be expected to fully devitrify during the compaction operation. Dynamic compaction of preheated material gave high density but poor strength, because of insufficient adhesion or particle cracking. Uniaxial pressing with some lateral flow to cause interparticle shear produced good densification and fair adhesion at moderate pressures, but only at temperatures far in excess of typical $T_g$ values (47) for this material. Similar temperatures were necessary to achieve satifactory density by slow forging (isothermal upsetting) of preforms warm pressed at 773 K.

No systematic attempt seems to have been made to indentify optimum"warm" consolidation conditions. Such an approach could be based on the hot consolidation maps developed by Arzt et al. (17). Such maps are shown for Metglas 2826 in figure 8 and 9 although it must be emphasized that available input data are too scanty to allow more than a demonstration of the principle.

The temperature dependence of flow stress of this alloy has been measured by Krenitsky and Ast (55), creep data have been determined by Gibeling and Nix (56), and incubation times for crystallization during creep deformation by Anderson and Lord (57). Unfortunately, the data pertain to

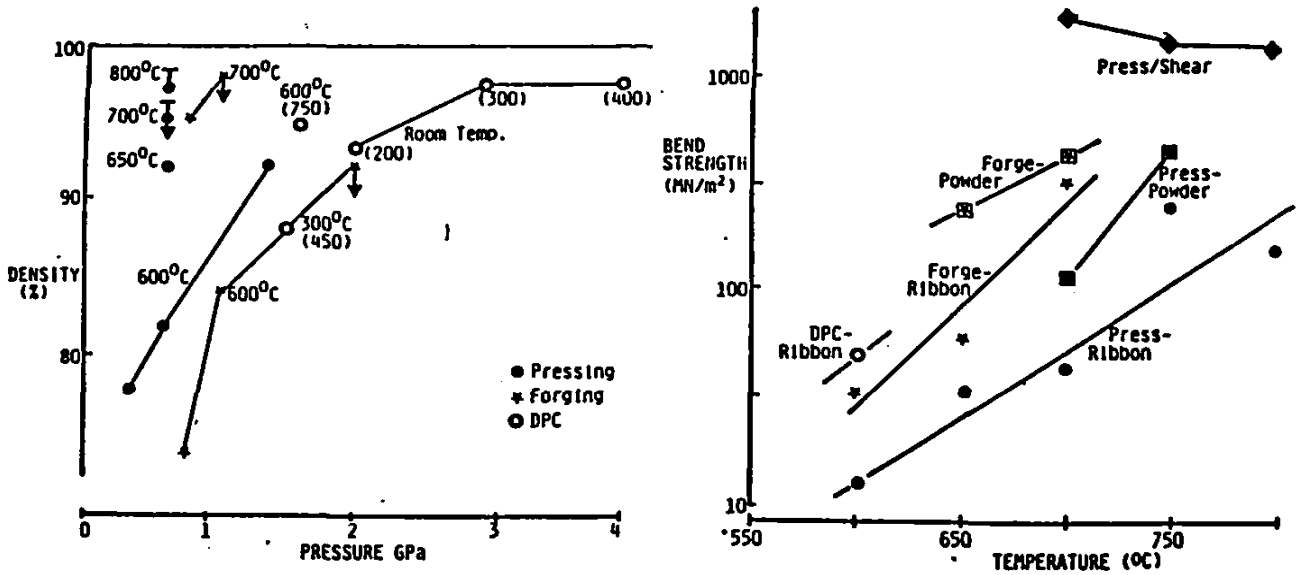


Figure 7: Density and strength achieved by various methods of hot compaction of originally amorphous $Ni_{70}-Si_{10}-B_{20}$ (41). Symbols not explained in figure inserts: DPC = dynamic compaction; bars above • = higher density obtained by pressing with shear flow; arrows below • = lower densities obtained when pressing powder instead of ribbons.

different temperatures, stresses and strains, necessitating considerable extrapolation in constructing a map. In particular, the creep and yield data were determined below $T_g$ (which for this alloy is at 643 K (58)), while the crystallization data were measured above $T_g$. The creep measurements at 523 - 573 K can be described in terms of a power law; their extrapolation beyond $T_g$ is at best a lower bound for the rate of time-dependent deformation in the upper region of the map shown in figure 9. Despite these reservations, the maps seem to reflect reality to a fair degree. Pressing ribbons of $Fe_{81.5}-B_{14.5}-Si_4$ at 600 K with .69 GPa for 600 s, Liebermann (47) reports a density of 75 % while the maps would predict 80 % for a spherical powder of $Fe_{40}-Ni_{40}-P_{14}-B_6$; similar agreement is found for ribbons of $Fe_{40}-Ni_{40}-B_{20}$.

At the right in figure 8, the map shows a field where the stresses are high enough to enforce densification by instantaneous yield. At lower stresses, to the left, only time-dependent deformation can effect densification. Density-pressure curves are shown for various times. At the temperature for which the diagram is constructed, the incubation time for crystallization is 3000 s. Times beyond that, i.e. the left part of the field, must be avoided.

At higher temperatures (figure 9), less pressure is required to produce full density by creep deformation, but crystallization will occur sooner. The disadvantage of shorter incubation times far outweighs the gain due to faster creep. Thus for essentially slow consolidation processes, like warm pressing or HIP, one should chose the lowest temperature compatible with a reasonable cycle time. This may appear surprising, but it is inevitable in the temperature range below the nose of the time-temperature-transformation plot. Empirical data are not available for higher temperatures, but calculations by Bergmann and Fritsch (59) indicate that the nose may be situated around 1000 K.

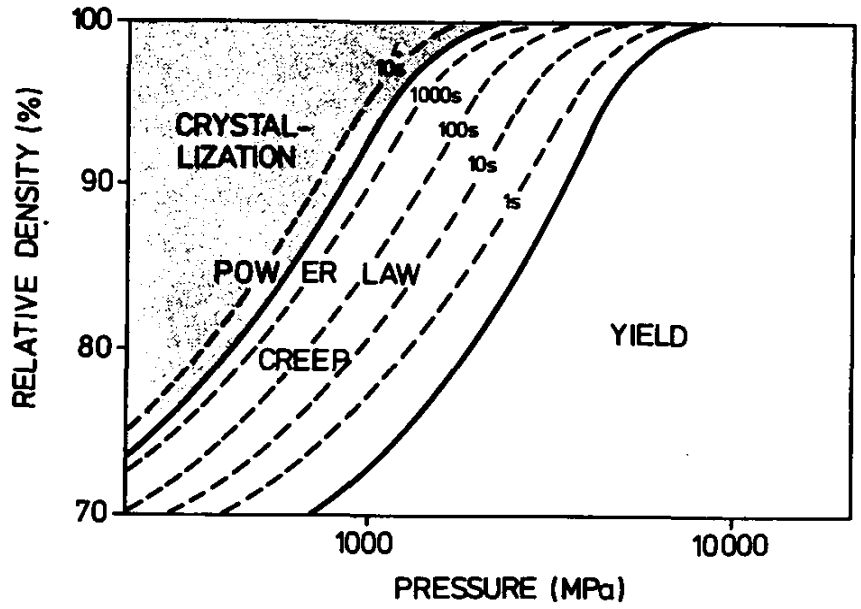


Figure 8: (Semi-hypothetical) map showing regions of instantaneous yield and "power law creep" for the compaction of Metglas 2826 ($Fe_{40}$-$Ni_{40}$-$P_{14}$-$B_6$) at 633 K. Also shown is the region where crystallization starts before full density has been reached.

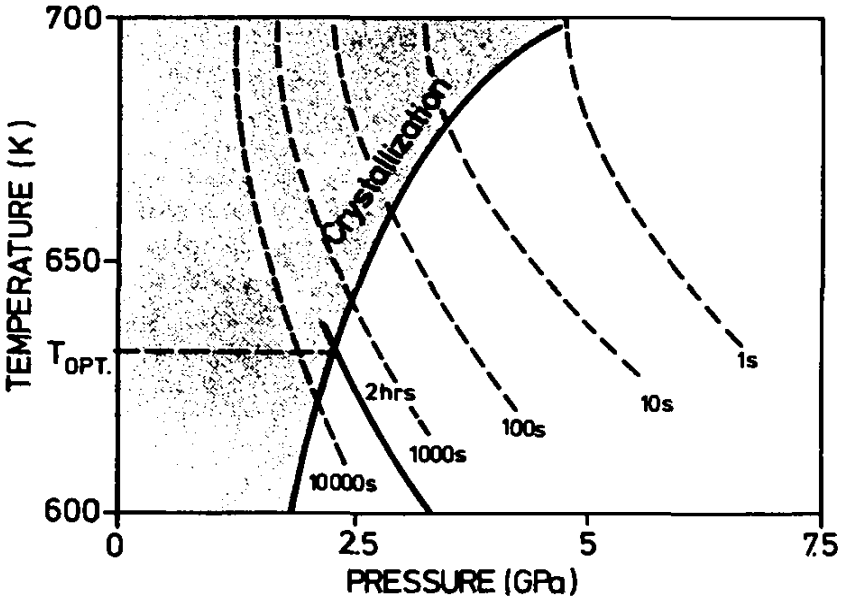


Figure 9: Minimum pressure to reach full density within stated times in warm compaction of Metglas (cf. figure 8), and region where crystallization intervenes before full densification. For a reasonable practical warm pressing time of 2 hrs, the optimum temperature (requiring minimum pressure) is 630 K.

Taken at face value, the maps in figures 8 and 9 indicate that most of the warm pressing experiments made so far used insufficient pressures and times. Pressures of the order of 2.5 GPa, the minimum indicated by figure 9, are beyond the reach of ordinary powder metallurgy dies, but they could easily be achieved in very simple belt-type apparatus. Relaxing the density requirement from 100 to 95 pct would reduce the pressure by about one-half, making it just manageable for conventional powder pressing dies (though still far beyond the present limit of HIP technology at about 0.2 GPa).

Let us now consider extrusion in the light of the maps. Since densification is fast, it has little to gain from thermally assisted deformation, and the required pressures must always be expected to be essentially higher than for slow pressing at equal temperature. Full densification has been reported at extrusion pressures of only 0.78 - 0.98 GPa at nominal temperatures of 640 - 660 K (47). In the light of figure 9, this would indicate substantially accelerated densification, which might have been due to adiabatic heating or to a beneficial effect of shear deformation. However, experience from powder forging (60) suggests that shear is beneficial mostly for bonding, not for densification. While shear may accelerate densification at low levels, it does not usually reduce the pressure requirement for reaching full density.

## 7. CONCLUDING REMARKS

Dynamic compaction with high velocity impact (gas gun or explosive) seems a promising but still somewhat problematic possibility for producing compact pieces of metastable materials. Open questions are:

- accurate control of energy input;
- reliable attainment of negligible porosity and good bonding, which both are mandatory for good mechanical properties;
- the narrow limits for heat input without property degradation;
- the feasibility of compacting pieces of large size and even moderately complex shapes.

Warm pressing is expected to require pressures which are clearly above the range of conventional die tooling, but manageable with simple high-pressure tooling. Bonding would be a problem in simple pressing, but probably not in isothermal forging which involves sufficient shear flow. The bonding problem could be greatly alleviated by fully inert processing and/or particle surface cleaning, as in present-day superalloy technology.

The warm consolidation maps presented in this paper suggest that all experiments made so far were considerably outside the optimum processing window.

Warm extrusion has already been proven feasible. The discussion in this paper suggests that experiments made so far may have been outside the optimum processing window, so that improvements could be expected.

To establish processing windows for warm forming operations, experimental work should be directed at

- determination of complete crystallization-time-temperature diagrams;
- the possible influence of simultaneous deformation on crystallization kinetics;
- "yield" data at high temperatures;
- "creep" data at high temperatures.

Such work should be worthwhile because the evidence suggests that the optimal processing parameters for warm-forming compact pieces of amorphous metallic alloys should be technically attainable, though requiring modifications of present-day forming equipment and powder handling methods.

## 8. REFERENCES


1. Bockstiegel G, Hewing J, Arch. Eisenhüttenw.,36, 1965, 751.
2. James PJ, Powder Metall. Internat., 4, 1972, 82, 145 and 193.
3. Kawakita K, Ludde KH, Powder Technol., 4, 1970/71, 61.
4. Arzt E, Fischmeister H, Mem. Sci. Rev. Metall.,76, 1979, 573.
5. Shapiro I, Kolthoff M, J. Phys. Colloid Chem., 51, 1947, 483.
6. Konopicky K, Radex-Rundsch,.3, 1948, 141.
7. Torre C, Berg- u. Hüttenm. Mh., 93, 1948, 62.
8. Heckel RW, Trans. AIME, 221, 1961, 1001.
9. Heliwell N, James PJ, Powder Metall. Internat., 7, 1973, 25.
10. James PJ, Powder Metall. Internat., 20, 1977, 21 and 199.
11. Sundström BO, Fischmeister H, Powder Metall. Internat.5, 1973, 171.
12. Fischmeister H, Arzt E, Olsson LR, Powder Metall., 21, 1978, 179.
13. Fischmeister H, Arzt E, Powder Metall., 26, 1983, 82.
14. Arzt E, Acta metall., 30, 1982, 1883.
15. Scott GD, Nature, 194, 1962, 956.
16. Fischmeister H, Arzt E, 7th Intern. Powder Metall. Conf., Dresden 1981, Vol. 1, 105.
17. Arzt E, Ashby MF, Easterling KE, Metall. Trans., 14A, 1983, 211.
18. Balzerowiak HP, Bock-Nussbaum F, Prümmer R, High Temp.-High Press., 3, 1971, 517.
19. Clyens S, Johnson W, Mater. Sci. Eng., 30, 1977, 121.
20. Lennon CRA, Bhalla AK, Williams JD, Powder Metall. 21, 1978, 29.
21. Gourdin WH, Mater. Sci. Eng., 67, 1984, 179.
22. Davis RF and Palmour H III, Journal of Materials Education (JEMMSE),5, 1, 1983, 151.
23. Davis RF, Horie Y, Scattergood RO, Palmour H III: Advances in Ceramics, Kingery WD, ed., Amer. Ceram. Soc., Columbus, 1984, 157.
24. Meyers MA, Gupta BB, Murr LE, J. Metals, 33, 1981, 21.
25. Raybould D, Morris DG, Cooper GA, J. Mater. Sci., 14, 1979, 2523.
26. Deutsches Patent No. 27 376 74.9.
27. Raybould D. Proc. 15th Intern. Machine Tool Res. and Design Conf., Tobias SA, Koenigsberger F. (Eds) MacMillan, London 1975, 627.
28. Morris DG, Met. Sci., 15, 1981, 116.
29. Kasiraj P, Vreeland T Jr, Schwarz RB, Ahrens TJ, Acta metall.,32,1984, 1235.
30. Campbell JD, Mater. Sci. Eng., 12, 1973, 3.
31. Raybould D, J. Mater. Sci., 16, 1981, 589.
32. Morris DG, Mater. Sci. Eng., 57, 1983, 187.
33. Crossland B, Williams JD, Metall. Rev., 15, 1970, 79.
34. Morris DG, Metal Science, 16, 1982, 457.
35. Morris DG, The Dynamic Compaction of Metal Powders, in "Metastable Crystalline Materials", MRS Boston 1983.
36. Roman OV, Bogdanov AP, Voloshin YuN, Gorobtsov VG, Pikus IM, Termich. Obrab. Metall., 10, 1983, 57.
37. Sargent PM, Ashby MF, Report CUED/C/MATS/TR. 98, March 1983, Cambridge University.
38. Buckley DH, Proc. 2nd Int. Conf. Sci. Hard Mater., Rhodes 1984, The Institute of Physics, Bristol, in press.
39. Pepper SV, J. Appl. Phys., 47, 1976, 801.

40. Bowden FP, Tabor D, Friction and Lubrication of Solids, Oxford University Press, London, 1950.
41. Morris DG: Compaction of Amorphous Ribbons and Powders. RQ5, 1984, Wurzburg.
42. Morris DG, Metal Sci., 14, 1980, 215.
43. Morris DG, J. Material Sci., 17, 1982, 1789.
44. Schwarz RB, Kasiraj P, Vreeland T Jr, Ahrens TJ, Acta metall., 32, 1984, 1243.
45. Fischmeister HF, Larsson LE, Powder Metall., 17, 1974, 227.
46. Morris DG, Metal Powder Report, 1983, p. 405.
47. Liebermann HH, Mater. Sci. Eng., 46, 1980, 241.
48. Pourahimi S, Thesis MS, Northeastern Univ., Boston, 1980, quoted in ref. 51.
49. Bruson A, Maloufi N, Mater. Sci. Eng., 64, 1984, L13.
50. Miller SA, Murphy RJ, in "Proc. 2nd Conf. Rapid Solid. Process.", Mehrabian R, Kear BH, Cohen M (Eds), Claitors, Baton Rouge, 1980,385.
51. Miller SA in "Amorphous Metallic Alloys", Luborsky FE (Ed), Butterworths, London, 1983, 506.
52. Stempin JL, Wexell DR, US Pat. 4 298 382, 1981, quoted in ref. 51.
53. Smith JS, Perepezko JH, Rasmussen DH, Loper Cr Jr, US Pat. 4 282 034, 1981.
54. Gibbs MRJ, Evetts JE, Shah NJ, J. Appl. Phys., 50, 1979, 7642.
55. Krenitsky DJ, Ast DG, J. Mater. Sci., 14, 1979, 275.
56. Gibeling JC, Nix WD, Scripta Met., 12, 1978, 919.
57. Anderson PM III, Lord AE, Jr., Mater. Sci. Eng., 44, 1980, 279.
58. Ast DG, Krenitsky DJ, Mater. Sci. Eng., 23, 1976, 241.
59. Bergmann HW, Fritsch HU, Metal Sci., 16, 1982, 197.
60. Fischmeister HF, Ann. Rev. Mater. Sci., 5, 1975, 151.